박사학위논문

(국문) 신경 교종 쥐 모델(GL261 glioma mouse model)을 대상으로 다양한 영상 검사 및 대사체학(metabolomics)을 이용한 종양의 대사 다양성에 대한 분석 및 고찰

(영문) Assessment of metabolic heterogeneity of tumor using various imaging modalities and metabolomics in GL261 glioma mouse model

울 산 대 학 교 대 학 원

의 학 과

이 철 민

신경 교종 쥐 모델(GL261 glioma mouse model)을 대상으로 다양한 영상 검사 및 대사체학(metabolomics)을 이용한 종양의 대사 다양성에 대한 분석 및 고찰

지 도 교 수 김 정 곤

이 논문을 박사학위 논문으로 제출함

2022년 8월

울 산 대 학 교 대 학 원

의 학 과

이 철 민

이 철 민 의 의학박사학위 논문을 인준함

심사위원 김 경 원 인

심사위원 김 호 성 인

심사위원 김 정 곤 인

심사위원 우 동 철 인

심사위원 조 경 구 인

울 산 대 학 교 대 학 원

2022년 8월

영문 요약

Objective: We tried to investigate the diverse tumor heterogeneity using various imaging modalities and metabolomic analysis.

Methods: We made a GL261 glioma mouse model in 7 male mice. Region-based analysis was performed by drawing region-of-interest (ROI)s in the tumor outer border and two-thirds of the tumor radius, dividing into tumor center and periphery. Transvsasular permeability (TP) was evaluated in dynamic-contrast-enhanced MRI (DCE-MRI) using an extravascular extracellular agent (Gd-DOTA), and blood volume (BV) was quantified using intravascular T2 agent (SPION). Diffusion of water molecules was evaluated in diffusion-weighted imaging (DWI), and glucose uptake was measured in ^{18}F-FDG PET as maximal standard uptake value (SUVmax). Immediately after imaging studies, glucose-mediated energy production was assessed by measuring the glycolysis and tricarboxylic acid (TCA) cycle activities, and glucose-mediated biosynthesis was evaluated by measuring the pentose phosphate pathway activity.

Results: The TP parameters (EnhRate and Washin) were higher in the tumor center than in the periphery ($p = 0.018$); however, the BV parameters (CBV and MVV) were higher in the tumor periphery than in the center ($p \leq 0.043$). The degree of diffusion restriction was higher in the tumor center than in the periphery ($p = 0.042$), and the ^{18}F-FDG uptake was also higher in the tumor center than in the periphery ($p = 0.018$). Among the glycolysis metabolites, FBP and 3PG were significantly higher in the tumor periphery than in the center (center to periphery ratio, 0.1–1.7 for FBP, 0.2–1.0 for 3PG, $p \leq 0.028$). In addition, CIT/ISO CIT of TCA cycle and S7P of pentose phosphate pathway were significantly higher in the tumor periphery than in the center (center to periphery ratio, 0.3–1.2 for CIT/ISO CIT and 0.2–0.9 for S7P, $p \leq 0.043$).

Conclusion: We demonstrated variable heterogeneities of the vasculature, diffusion, and metabolism between the tumor center and periphery.

차례

Introduction

Tumor heterogeneity is an important emerging concept in the current anti-cancer treatment and resistance. Tumor heterogeneity encompasses various aspects of cancer cells, including gene expression, metabolism, morphology, proliferation, and metastasis. It can occur between tumors (inter-tumor heterogeneity) and within tumors (intra-tumor heterogeneity) (1). Various types of cancers reported heterogeneity in the genetic, metabolic, and cellular levels. These heterogeneities assist cancer progression, evasion from chemotherapy, recurrence, and metastasis. Increased knowledge about tumor heterogeneity could be an important guide for the more refined anti-cancer treatment strategies (2).

Heterogeneity of the tumor vasculature was reported in a previous study on the glioma mouse model (3). There was heterogeneity of tumor vasculature between the tumor center and periphery, and the heterogeneities were more pronounced during the tumor growth. Furthermore, the different tumor vasculatures between the tumor center and periphery made different anti-angiogenic treatment responses.

Tumor vasculature through neo-angiogenesis plays a complementary role in tumor metabolism by supplying nutrients and oxygen to tumor tissue. Tumor metabolism is complex, and it is composed of a variety of metabolic processes. Upregulation of glycolysis in the abundant oxygen environment is a well-known feature of the tumor called the ‘Warburg effect (aerobic glycolysis)’ (4). The tricarboxylic acid cycle (TCA cycle) produces energy in the form of GTP, and NADH is another product of the TCA cycle, which decreases oxygen stress in the tumor tissue (reducing agent). The pentose phosphate pathway (PPP) produces many building blocks of nucleic acids, amino acids, and fatty acids, which help the proliferation of tumor cells.

Magnetic resonance imaging (MRI) is an excellent tool for evaluating tissue characteristics, and various MRI techniques and contrast agents added to conventional MRI sequences could detect discriminating features of the tumor tissue. For example, the diffusion-weighted image (DWI) measures the mobility of water molecules in the specific tissue, which provides information about

cellular density and vascular flow of tissue. Diffusion restriction is a well-known feature of malignant tumors (5, 6). Furthermore, tumor tissue's transvascular permeability could be evaluated using extracellular contrast agents (e.g., small-molecular gadolinium chelates) and blood volume using intravascular contrast agents (e.g., superparamagnetic iron oxide nanoparticles). In addition, ^{18}F-FDG PET could also evaluate the tissue glucose uptake, and malignant tumors usually show increased ^{18}F-FDG uptake (7). To our knowledge, few studies have simultaneously evaluated various tumor heterogeneities using various imaging modalities. Furthermore, 'metabolomics' deals with various chemical processes and metabolites in cells, tissues, organs, or organisms. We could evaluate specific metabolic processes in the tissue and acquire the readout of the physiological states of the tissue (8).

Therefore, our study aimed to evaluate diverse tumor heterogeneities within the GL261 glioma mouse model using various imaging modalities and metabolomics analysis of tumor tissue.

Materials and Methods

Brain tumor model and study protocol

In 7 male mice (Balb/c, 8-week old, weight 24-26 g), GL261 glioma cells (Korean Cell Line Bank, Seoul, Korea) were injected into the right cerebral hemisphere using a stereotaxic injection kit (Hamilton Co, NV, USA). Skull holes were generated 1-mm inferior and 2.5-mm lateral to the bregma. Thereafter, tumor cells (1.2×10^5 cells) were injected slowly over a period of 4 minutes to the level 2.2 mm below the dura.

MRI, ^{18}F-FDG PET and co-registration

Detailed information about the imaging sequence and measurement method of imaging parameters is presented in Supplementary. MRI parameters were acquired using a 7.0 T Bruker pre-clinical MRI scanner (PharmaScan 70/16, Brucker BioSpin GmbH, Germany), which included a T2-weighted image (T_2WI), apparent diffusion coefficient (ADC) image from diffusion-weighted image (DWI), dynamic contrast-enhanced MRI (DCE-MRI), and R_2^* and R_2 maps. ^{18}F-FDG PET was obtained after MRI using the nanoScanPET/MRI system (1T, Mediso, Hungary), which provided the standard uptake value (SUV).

Tumor volume change was monitored in T2-weighted images (T_2WIs) acquired every 3 days after tumor cell injection. When the tumor volume reached approximately 10 mm^3 (approximately 4 days after tumor inoculation), tumor characteristics were evaluated in MRI and PET.

The tumor vasculature was quantified by measuring transvascular permeability (TP) and blood volume (BV) in MRI (9). TP was estimated in DCE-MRI using an extracellular-fluid contrast agent (Dotarem®, Guerbet, France; molecular weight, 500 D; injection dose, 0.1 mL/kg of body weight). BV was measured by quantifying the R_2^* and R_2 changes (i.e., ΔR_2^* and ΔR_2) induced by intravascular susceptibility contrast agent (superparamagnetic iron oxide nanoparticles (SPION); core diameter, 5 nm to 10 nm; hydrostatic diameter, 20 ± 5 nm; 1 mg of iron per 1 milliliter of SPION solution; injection dose, 30 mg Fe/kg bodyweight)) (10). Prior to intravenous CA injection, T_2WIs

were acquired using the fast-spin echo sequence. DCE-MRI was thereafter performed before and after manual bolus injection of Gd-DOTA (30 seconds after scanning start) through the tail vein. SPION-induced ΔR_2^* and ΔR_2 were measured after DCE MRI examinations. After MRI examination, the mice were transferred to the PET-MRI unit while being kept anesthetized. ^{18}F-FDG PET was obtained before MRI using the nanoScanPET/MRI system (1T, Mediso, Hungary).

Image parameters were quantified using the Analysis of Functional NeuroImages (AFNI, National Institute of Health, Bethesda, MD, USA) program and ImageJ (National Institute of Health). Using the T_2WI as a reference frame, all MRI and ^{18}F-FDG PET parameter maps were co-registered and interpolated to achieve the same voxel geometry.

Imaging parameter measurement

An experienced radiologist drew regions of interest (ROIs) on T_2WI, including tumor center, tumor periphery and peritumoral brain tissue; areas with T2-hyperintensity and Gd enhancement were considered the outer border of tumor tissue. By referring to previous studies that described the active proliferation and angiogenesis in tumor border, the outer one-third of the tumor area was assigned as the periphery and the other area as the center (3, 11). After drawing the ROI covering the entire tumor area, the radiologist drew another ROI that passed through two-thirds of the tumor radius. The inner area of this ROI was considered as the tumor center and the outer area as the tumor periphery. The area of ROI in peritumoral brain tissue was set to be equal to that of the tumor center.

TP parameters were quantified using a non-PK-model-based analysis of DCE-MRI. To minimize machine- or sequence-induced variations, the time-intensity curve was normalized by dividing the signal intensity at each time point with the mean pre-contrast signal intensity. Thereafter, the maximum enhancement rate (EnhRate) (maximum signal intensity/mean pre-contrast signal intensity) and initial area under the curve (Washin) over 60 seconds were measured. For measuring BV parameters, pre- and post-SPION R_2^* and R_2 values were calculated according to the following equation:

$$SI = M_0 \cdot e^{-R_2(^*) \cdot t}$$

Where SI is the MR signal intensity, M_0 is the proton density, t is the echo time, and R_2 (*) is the transverse relaxation rate. The relative BV weighted for macrovascular (CBV, cerebral blood volume) and microvascular blood vessels (MVV, microvascular volume) was determined as SPION-induced ΔR_2^* and ΔR_2, respectively (12, 13). In ^{18}F-FDG PET, the standard uptake value (SUV) was measured.

Biochemical and metabolomic assays

Immediately after the imaging examination, a solution of 2% Evans blue (EB, 4 ml/kg, Sigma, USA) was intravenously injected and circulated for 30 min. After animals were euthanized by cervical dislocation, the brains were quickly removed and embedded in stainless steel brain matrices cutting template (Kent Scientific, Torrington, CT, USA). The mid-coronal slices of EB-stained brian tumor were obtained. Thereafter, tumor center, tumor periphery and peritumoral tissue were obtained by referring to the MRI imaging (Figure 1).

To obtain metabolic characteristics of tumor at a molecular level, glucose-mediated energy production and glucose-mediated biosynthesis were estimated using LC-MS/MS system equipped with 1290 HPLC, Qtrap 5500, and a reverse-phase column (Synergi Fusion-RP 50 × 2 mm; Phenomenex, Torrance, CA, USA). Detailed information on biochemical and metabolomic assays is described in Supplementary. Glucose-mediated energy production was assessed by measuring the glycolysis and tricarboxylic acid (TCA) cycle activities (14). Glucose-mediated biosynthesis was evaluated by the pentose phosphate pathway activity, as it contributes to fatty acid, nucleotide, nucleic acid, and aromatic amino acid synthesis (15).

Statistical Analysis

The Wilcoxon-singed rank test was used to compare each parameter between the tumor center and periphery. A p-value of < 0.05 was considered statistically significant. Statistical analysis was performed using SPSS version 26.0 statistical software (IBM, Armonk, NY).

Figure 1. Gross (A, B) and histopathology (C) specimen in a representative mouse brain.

Results

Tumor heterogeneity in MRI and PET

1) Vasculature

There were heterogeneities of tumor vasculature between the tumor center and periphery. The TP parameters (EnhRate and Washin) were significantly higher in the tumor center than the tumor periphery (center to periphery ratio, 1.6–7.4 for Enh and 1.0–4.7 for Washin, $p = 0.018$). On the contrary, the BV parameters (CBV and MVV) were significantly higher in the tumor periphery than in the tumor center (center to periphery ratio, 0.4–1.1 for CBV and 0.1–1.2 for MVV, $p \leq 0.043$) (Table 1 and Figure 2).

2) Diffusion of water molecule

In the DWI, the tumor center and periphery showed a difference in the diffusion restriction. The median ADC value was significantly higher in the tumor periphery than in the center (center to periphery ratio, 0.8–1.1, $p = 0.042$). In other words, the degree of diffusion restriction was significantly higher in the tumor center than in the tumor periphery (Table 1 and Figure 2).

3) Glucose uptake

Tumor heterogeneity was also observed in the ^{18}F-FDG PET. The tumor center showed a median SUVmax of 220.0 (range, 166.0–247.0) and the tumor periphery showed a median SUVmax of 184.0 (range, 152.0–205.0). The median SUVmax was significantly higher in the tumor center than in the tumor periphery (center to periphery ratio, 1.1–1.4, $p = 0.018$). This means that the tumor center showed a higher glucose uptake rate than the tumor periphery (Table 1 and Figure 2).

Table 1. Comparison of center, periphery, and control for each imaging parameter

Data are the median (range) of variables.

	Center (C)	Periphery (P)	Control (N)	Center to periphery ratio (C/P)	*p* value*
Enh	0.446 (0.254–1.545)	0.160 (0.096–0.310)	0.095 (0.085–0.142)	1.6–7.4	0.018
Washin	1486.0 (976.0–2244.0)	641.0 (362.9–2226.0)	1028.0 (266.0–1288.0)	1.0–4.7	0.018
CBV	92.0 (68.0–140.0)	136.5 (103.9–208.0)	129.0 (78.0–199.9)	0.4–1.1	0.028
MVV	2.8 (1.0–10.8)	7.9 (5.0–11.7)	10.8 (8.7–14.9)	0.1–1.2	0.043
ADC	0.460 (0.388–0.651)	0.535 (0.423–0.668)	0.492 (0.365–0.555)	0.8–1.1	0.042
SUV	220.0 (166.0–247.0)	184.0 (152.0–205.0)	135.0 (70.0–162.0)	1.1–1.4	0.018

*P-value of comparison between the center (C) and periphery (P).

Figure 2. Magnetic resonance imaging (MRI) and ^{18}F-FDG positron emission tomography (PET) results in a representative mouse brain. The EnhRate (B) and Washin (C) were significantly higher in the tumor center than in the tumor periphery. On the contrary, CBV (D) and MVV (E) were significantly higher in the tumor periphery than in the tumor center. In the ADC (F), the tumor center showed a higher ADC value than the periphery. The tumor center showed higher ^{18}F-FDG uptake in ^{18}F-FDG PET (G).

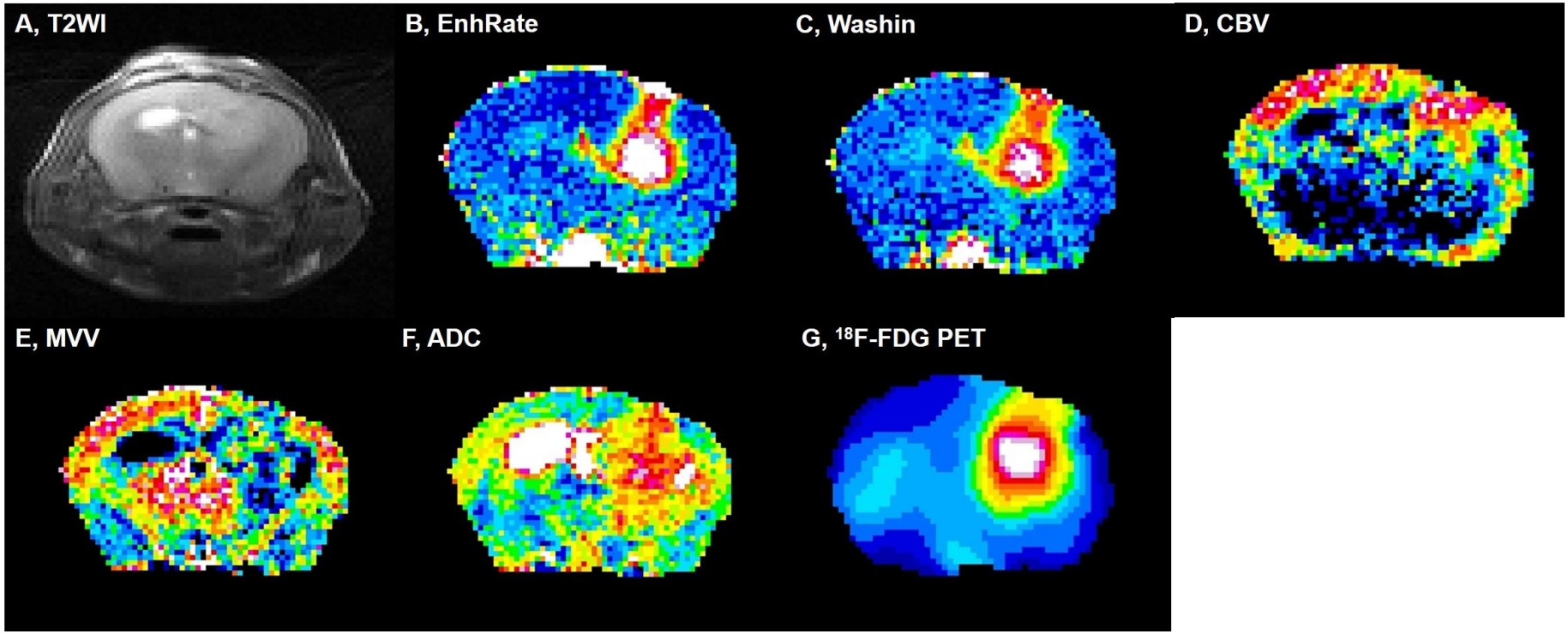

Tumor heterogeneity in metabolomics

1) Glycolysis

The heterogeneity of glycolysis metabolites was noted in the metabolomic analysis between the tumor center and periphery. The median FBP and 3PG levels were significantly higher in the tumor periphery than in the center (center to periphery ratio, 0.1–1.7 for FBP, 0.2–1.0 for 3PG, $p \leq 0.028$). However, other glycolysis metabolites (including GLC, G6P/F6P, PEP, LAC, and PYR) showed were higher in the tumor periphery than in the center without the statistically significant differences ($p \geq 0.091$) (Table 2 and Figure 3).

2) TCA cycle

The median CIT/ISO CIT level was significantly higher in the tumor periphery than in the center (center to periphery ratio 0.3–1.2; $p = 0.043$). The AKG, FUM, SUC, and NAD were higher in the tumor center than in the periphery, and the MAL and NADH were higher in the periphery than in the center, without statistically significant differences between the tumor center and periphery ($p \geq 0.063$).

3) Pentose phosphate pathway

Among the pentose phosphate pathway metabolites, the median S7P level was significantly higher in the tumor periphery than in the center (center to periphery ratio, 0.2–0.9, $p = 0.018$). The median R5P, R15BP, and 6PG levels were also higher in the tumor periphery than in the center, which was not statistically significant ($p \geq 0.091$) (Table 2 and Figure 3).

Table 2. Comparison of center, periphery, and control for each metabolite

	Center (C)	Periphery (P)	Control (T)	Center to periphery ratio (C/P)	*p* value[†]
GLC	6.433 (3.855–11.088)	10.079 (1.812–21.536)	6.237 (3.835–10.995)	0.5–2.1	0.128
G6P/F6P	0.242 (0.146–0.449)	0.301 (0.111–3.090)	6.237 (3.835–10.995)	0.1–1.4	0.091
FBP	0.021 (0.009–0.058)	0.064 (0.008–0.500)	0.044 (0.010–0.074)	0.1–1.7	0.028
3PG	0.079 (0.054–0.172)	0.119 (0.072–0.850)	0.135 (0.069–0.266)	0.2–1.0	0.018
PEP	0.005 (0.003–0.010)	0.005 (0.002–0.025)	0.006 (0.004–0.008)	0.4–1.8	0.176
LAC	31.285 (19.614–60.415)	40.382 (9.962–132.022)	34.392 (22.526–54.286)	0.5–2.0	0.176
PYR	0.254 (0.151–0.469)	0.327 (0.080–1.182)	0.262 (0.178–0.440)	0.4–1.9	0.128
CIT/ISO CIT	1.349 (0.309–1.959)	2.911 (0.490–6.187)	2.160 (0.924–3.472)	0.3–1.2	0.043
AKG	0.814 (0.569–1.513)	0.461 (0.232–2.154)	0.348 (0.254–0.558)	0.7–2.4	0.237
FUM	1.907 (1.027–3.254)	1.822 (0.743–5.674)	1.554 (1.469–1.887)	0.6–1.5	0.866
MAL	9.018 (3.814–14.404)	10.444 (4.100–31.086)	9.069 (8.008–11.799)	0.5–1.3	0.237
SUC	4.940 (2.958–6.808)	4.387 (0.870–16.629)	5.172 (0.885–6.416)	0.4–3.4	0.237
NAD	1.125 (0.590–2.218)	0.889 (0.165–2.491)	0.578 (0.187–0.921)	0.9–5.0	0.063
NADH	0.015 (0.005–0.022)	0.017 (0.000–0.033)	0.009 (0.001–0.012)	0.7–49.9	1.000

R5P	0.381 (0.140–0.659)	0.396 (0.193–1.708)	0.512 (0.346–0.961)	0.4–1.1	0.091
R15BP	0.004 (0.001–0.007)	0.006 (0.002–0.014)	0.005 (0.003–0.008)	0.3–1.2	0.176
S7P	0.065 (0.024–0.096)	0.172 (0.041–0.404)	0.203 (0.059–0.345)	0.2–0.9	0.018
6PG	0.041 (0.013–0.063)	0.045 (0.014–0.152)	0.044 (0.034–0.059)	0.4–1.3	0.176
NADP	0.013 (0.004–0.016)	0.013 (0.003–0.022)	0.009 (0.005–0.015)	0.6–1.8	1.000
AMP	8.746 (2.838–12.586)	11.481 (1.793–15.468)	7.410 (4.252–16.017)	0.6–1.9	0.735
ADP	0.218 (0.075–0.284)	0.216 (0.049–0.468)	0.157 (0.076–0.187)	0.5–2.0	0.612
ATP	0.006 (0.003–0.012)	0.008 (0.002–0.027)	0.007 (0.004–0.008)	0.4–3.3	0.237

Data are the median (range) of variables.

*P-value of comparison between the center (C) and periphery (P).

Figure 3. Metabolomic and biochemical analysis results in mouse brain. (A) The median FBP and 3PG levels in glycolysis were significantly higher in the tumor periphery than in the center. (B) In the tricarboxylic acid (TCA) cycle, the median CIT/ISO CIT level was significantly higher in the tumor periphery than in the center. (C) Among the metabolite of the pentose phosphate pathway (PPP), the S7P level was significantly higher in the tumor periphery than in the center.

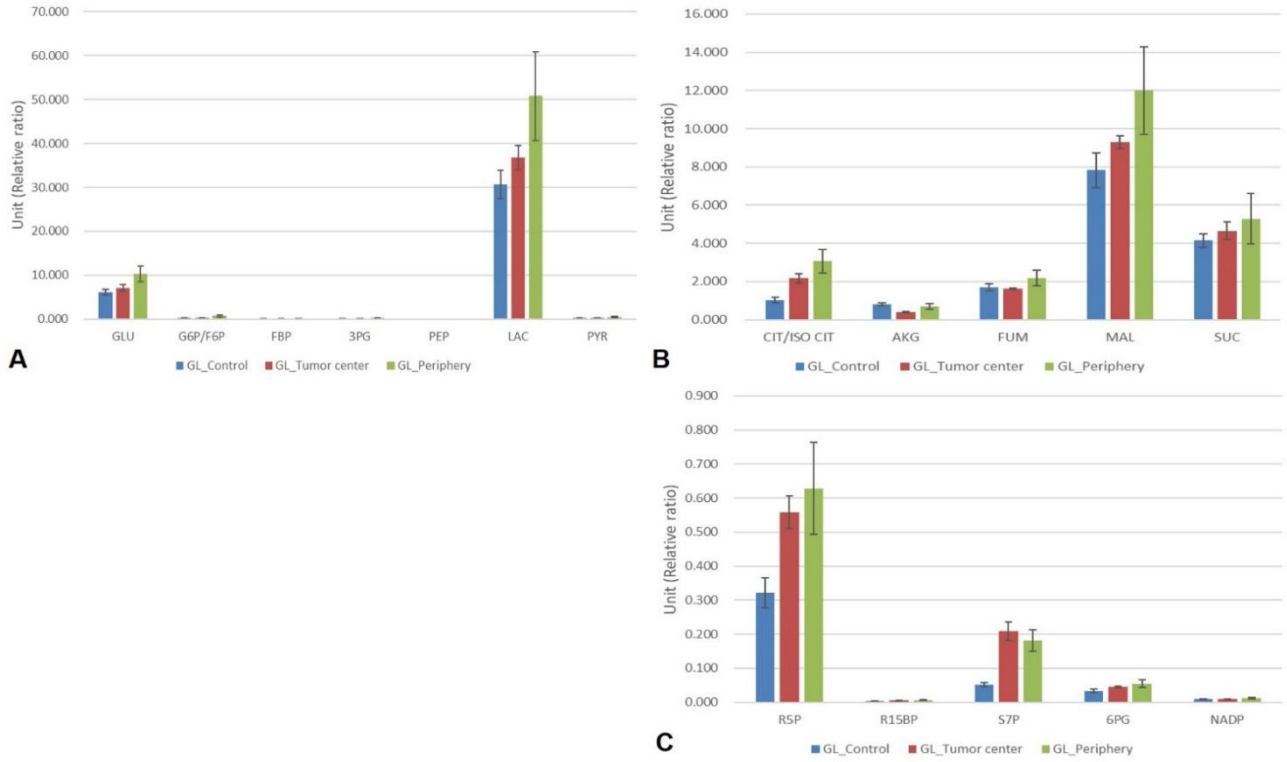

Discussion

Our study showed variable heterogeneities between the tumor center and periphery. The TP parameters were higher in the tumor center than in the periphery; however, the BV parameters were higher in the tumor periphery than in the center. In addition, the degree of diffusion restriction was higher in the tumor center than in the periphery, and the ^{18}F-FDG uptake was also higher in the tumor center than in the periphery. Among the glycolysis metabolites, FBP and 3PG were significantly higher in the tumor periphery than in the center. In addition, CIT/ISO CIT of the TCA cycle and S7P of the PPP were significantly higher in the tumor periphery than in the center.

The heterogeneity of tumor vasculature is well-known through a previous study (3). The highly active VEGF expression in the tumor periphery increases neoangiogenesis and vascular stabilization, contributing to invasive cancer margin (16, 17). The upregulated, less-leaky vessel formation in the tumor periphery increased BV parameters in the tumor periphery more than in the center. On the contrary, the lack of angiogenesis stimulation in the tumor center results in vascular regression and progressive disengagement of endothelial cells. Therefore, the plasma-to-interstitium flux increases, increasing TP parameters (18).

The degree of diffusion restriction in DWI was higher in the tumor center than in the periphery. The DWI reflects the mobility of water molecules in the intracellular and extracellular space of tumor tissue, and the tissue cellularity also contributes to the DWI signal intensity (5, 6). Because there was no difference in the cellularity between the tumor center and periphery in histopathology, the difference in the diffusion restriction might be affected by the mobility of water molecules in the tumor tissue. The vascular stabilization in the tumor periphery by the neoangiogenesis might increase the mobility of water molecules. On the contrary, the vascular regression in the tumor center because of the lack of neoangiogenesis might decrease the water molecule flow, resulting in the signal increase in the DWI.

There was heterogeneity of ^{18}F-FDG uptake and glycolysis metabolites between the tumor center and the periphery. The ^{18}F-FDG uptake was higher in the tumor center than in the periphery.

^{18}F-FDG is a glucose analog taken up by metabolically active tumor cells through glucose transporter (GLUT) of the cell membrane, and then ^{18}F-FDG is phosphorylated by hexokinase (HK) like glucose. However, unlike phosphorylated glucose (G-6-P), phosphorylated ^{18}F-FDG (FDG-6-P) cannot undergo further glycolysis and might be entrapped within the cell. We could detect the level of entrapped FDG-6-P in the PET as SUVmax (7). Many cancer cells show GLUT dysregulation and sustained glucose uptake (19). Thus, the higher SUVmax in the tumor center means a higher glucose uptake via GLUT in the tumor center than in the periphery. In the subsequent analysis of glycolysis metabolites, FBP and 3PG were higher in the tumor periphery than in the center. The higher ^{18}F-FDG uptake and lower glycolysis metabolites in the tumor center are conflicting results. This conflicting result might be because the tumor center was mostly undergoing aerobic glycolysis, which might need more glucose uptake because of the low efficacy of glycolysis; therefore, the GLUT is more activated in the tumor center than in the periphery. However, the absolute rate of glycolysis might be higher in the tumor periphery than in the center, resulting in higher glycolysis metabolites in the tumor periphery. The active glycolysis rate in the tumor periphery might elevate the lactate level, inducing acidification of the tumor microenvironment and facilitating tumor aggressiveness.

There was also heterogeneity of TCA cycle metabolites between the tumor center and the periphery. Among the TCA cycle metabolites, CIT/ISO CIT was significantly higher in the tumor periphery than in the center. However, there were no statistically significant differences between the tumor center and periphery, even though there were trends in differences between the center and periphery according to the metabolites. The alteration of the TCA cycle by the interaction between mitochondrial dysfunction and hypoxia-induced factor (HIF) is well-known through previous literature (20, 21). The isocitrate dehydrogenase 2 (IDH2) mutation fails to convert ISO CIT to AKG, and the mutation in the malate dehydrogenase 2 (MDH2) causes the accumulation of malate. Furthermore, fumarate and succinate might accumulate because of the mutations in the fumarate hydrogenase (FH) and succinate dehydrogenase (SDH), respectively. These mutations of TCA cycle enzymes also contribute to the inhibition of pyruvate dehydrogenase (PHD), resulting in the failure to

convert pyruvate to Acetyl-CoA and contributing to the stabilization of the HIF signaling pathway and target genes (22, 23). In our study, the different levels of TCA cycle metabolites might mean the heterogeneity in the mitochondrial dysfunction between the tumor center and periphery; some enzymes might have more mutations in the center, and others might have more mutations in the tumor periphery.

The PPP also showed heterogeneity between the tumor center and the periphery. Among the PPP metabolites, S7P was significantly higher in the tumor periphery than in the tumor center, and other PPP metabolites also showed higher trends in the tumor periphery than in the center without statistically significant differences. This might be because the tumor periphery might be more actively undergoing the PPP than the center, and PPP metabolites are essential building blocks for the biosynthesis of nucleotides and nucleic acids. This increased biosynthesis might assist the tumor proliferation and invasiveness in the tumor periphery.

There may be an issue raised regarding the influence of Gd-DOTA on the measurement of SPION-induced ΔR2* and ΔR2. Because Gd-DOTA has a short plasma half-life (approximately ~ 30 minutes) and a significantly low R_2 relaxivity (4.17 mmol/L/s) compared with our SPION (40 mmol/L/s) (24), residual gadolinium after DCE-MRI examination would not affect SPION-induced ΔR_2^* and ΔR_2 measurements.

There are some limitations to our study. First, we evaluated tumor heterogeneity in the GL261 glioma in mice. However, there might be a difference in the tumor heterogeneity according to the tumor cell type, and the result of our study could not be applied to all solid tumors. Second, the region-based analysis might have the issue of subjectiveness. However, most comparisons showed apparent differences between the tumor center and periphery. Finally, we evaluated the metabolic changes at the cellular level, not at the mitochondrial level. In addition, compared to imaging parameters, only a few metabolic parameters showed statistical differences between the tumor center and periphery. However, since metabolic analyses were performed in microgram units, trivial variables might have affected the tumor center and periphery difference. In addition, the small number

of mice also might have limited the verification of statistical significance between the tumor center and periphery.

Conclusion

In conclusion, our study demonstrated variable heterogeneities of the vasculature, diffusion, and metabolism between the tumor center and periphery. The increased knowledge of variable tumor heterogeneities might improve the anti-cancer therapy by introducing new targeting agents or combining pre-existing agents.

참고문헌 목록

1. Marusyk A, Polyak K. Tumor heterogeneity: Causes and consequences. Biochim Biophys Acta 2010;1805:105-117
2. Reiter JG, Makohon-Moore AP, Gerold JM, Heyde A, Attiyeh MA, Kohutek ZA et al. Minimal functional driver gene heterogeneity among untreated metastases. Science 2018;361:1033-1037
3. Kim C, Suh JY, Heo C, Lee CK, Shim WH, Park BW et al. Spatiotemporal heterogeneity of tumor vasculature during tumor growth and antiangiogenic treatment: Mri assessment using permeability and blood volume parameters. Cancer Med 2018;7:3921-3934
4. Abdel-Wahab AF, Mahmoud W, Al-Harizy RM. Targeting glucose metabolism to suppress cancer progression: Prospective of anti-glycolytic cancer therapy. Pharmacol Res 2019;150:104511
5. Hamstra DA, Rehemtulla A, Ross BD. Diffusion magnetic resonance imaging: A biomarker for treatment response in oncology. J Clin Oncol 2007;25:4104-4109
6. Koh DM, Collins DJ. Diffusion-weighted mri in the body: Applications and challenges in oncology. AJR Am J Roentgenol 2007;188:1622-1635
7. Kapoor V, McCook BM, Torok FS. An introduction to pet-ct imaging. Radiographics 2004;24:523-543
8. Hollywood K, Brison DR, Goodacre R. Metabolomics: Current technologies and future trends. Proteomics 2006;6:4716-4723
9. Kim JH, Suh JY, Woo DC, Sung YS, Son WC, Choi YS et al. Difference in the intratumoral distributions of extracellular-fluid and intravascular mr contrast agents in glioblastoma growth. NMR Biomed 2016;29:1688-1699
10. Stark DD, Weissleder R, Elizondo G, Hahn PF, Saini S, Todd LE et al. Superparamagnetic iron oxide: Clinical application as a contrast agent for mr imaging of the liver. Radiology

1988;168:297-301

11. Brú A, Albertos S, Luis Subiza J, García-Asenjo JL, Brú I. The universal dynamics of tumor growth. Biophys J 2003;85:2948-2961

12. Farrar CT, Kamoun WS, Ley CD, Kim YR, Kwon SJ, Dai G et al. In vivo validation of mri vessel caliber index measurement methods with intravital optical microscopy in a u87 mouse brain tumor model. Neuro Oncol 2010;12:341-350

13. Troprès I, Grimault S, Vaeth A, Grillon E, Julien C, Payen JF et al. Vessel size imaging. Magn Reson Med 2001;45:397-408

14. Kim HJ, Kim SJ, Woo CW, Kim ST, Im M, Park SK et al. Treatment of chemotherapy-induced cachexia with bst204: A multimodal validation study. Metabolomics 2021;17:36

15. Stincone A, Prigione A, Cramer T, Wamelink MM, Campbell K, Cheung E et al. The return of metabolism: Biochemistry and physiology of the pentose phosphate pathway. Biol Rev Camb Philos Soc 2015;90:927-963

16. Bartha K, Rieger H. Vascular network remodeling via vessel cooption, regression and growth in tumors. J Theor Biol 2006;241:903-918

17. Carmeliet P, Jain RK. Angiogenesis in cancer and other diseases. Nature 2000;407:249-257

18. Hardee ME, Zagzag D. Mechanisms of glioma-associated neovascularization. Am J Pathol 2012;181:1126-1141

19. Kim YH, Jeong DC, Pak K, Han ME, Kim JY, Liangwen L et al. Slc2a2 (glut2) as a novel prognostic factor for hepatocellular carcinoma. Oncotarget 2017;8:68381-68392

20. Porporato PE, Filigheddu N, Pedro JMB, Kroemer G, Galluzzi L. Mitochondrial metabolism and cancer. Cell Res 2018;28:265-280

21. Chiu HY, Tay EXY, Ong DST, Taneja R. Mitochondrial dysfunction at the center of cancer therapy. Antioxid Redox Signal 2020;32:309-330

22. Bian Y, Li L, Dong M, Liu X, Kaneko T, Cheng K et al. Ultra-deep tyrosine phosphoproteomics enabled by a phosphotyrosine superbinder. Nat Chem Biol 2016;12:959-

966

23. Bao X, Zhang J, Huang G, Yan J, Xu C, Dou Z et al. The crosstalk between hifs and mitochondrial dysfunctions in cancer development. Cell Death Dis 2021;12:215

24. Guilfoyle DN, Dyakin VV, O'Shea J, Pell GS, Helpern JA. Quantitative measurements of proton spin-lattice (t1) and spin-spin (t2) relaxation times in the mouse brain at 7.0 t. Magn Reson Med 2003;49:576-580

국문 요약

목적: 우리는 다양한 영상 검사와 대사체학 (metabolomics)를 이용하여 종양의 중심부와 주변부의 대사 다양성을 분석하고자 하였다.

대상 및 방법: 7 마리의 수컷 쥐를 이용하여 GL261 뇌교종 모델을 만들었고 종양 반지름의 3 분의 2 에 해당하는 지점에서 종양을 중심부와 주변부로 나누었다. 혈관내 투과성 지표는 혈관외세포제 (Gd-DOTA)를, 혈액량 지표는 혈관내작용제제 (SPION)를 사용하여 역동적 조영 증강 영상 (DCE-MRI)을 시행하여 이미지를 획득하고 각각의 지표를 정량화 하였다. 확산강조영상 (DWI)에서 물 분자의 확산 정도를 평가하였으며, 양전자 방출 단층촬영 (^{18}F-FDG PET)을 이용하여 포도당 흡수 정도를 최대 표준섭취계수 (SUVmax)로 측정하였다. 영상 검사 직후 해당 과정 (Glycolysis)과 시트르산 회로 (TCA cycle) 대사 산물을 측정하여 포도당 매개 에너지 생산을 평가하였고, 오탄당 인산 경로 (pentose phosphate pathway) 대사 산물을 측정하여 포도당 매개 생합성을 평가하였다.

결과: 혈관내 투과성 지표 (EnhRate 및 Washin)는 종양 주변부보다 종양 중심부에서 더 높았고 ($p = 0.018$), 혈액량 지표 (CBV 및 MVV)는 주변부보다 중심부에서 더 높았다 ($p \leq 0.043$). 물 분자의 확산 억제 정도는 주변부보다 중심부에서 더 높았고 ($p = 0.042$), 포도당 흡수 정도도 주변부보다 중심부에서 더 높았다 ($p = 0.018$). 해당 과정 대사산물

중 FBP 와 3PG 는 종양 주변부에서 중심부보다 유의하게 높았다 (center to periphery ratio, 0.1–1.7 for FBP, 0.2–1.0 for 3PG, $p \leq 0.028$). 또한 시트르산 회로 대사산물인 CIT/ISO CIT 와 오탄당 인산 경로 대사산물인 S7P 모두 종양 주변부가 중심부보다 유의하게 높았다 (center to periphery ratio, 0.3–1.2 for CIT/ISO CIT, 0.2–0.9 for S7P, $p \leq 0.043$)

결론: 본 연구를 통하여 종양의 중심부와 주변부 간의 혈관, 확산 및 대사의 다양성을 입증할 수 있었다.